The Astrophysical Journal, 616:1181–1187, 2004 December 1

H_2 IMAGING OF THREE PROTO–PLANETARY AND YOUNG PLANETARY NEBULAE[1]

Kevin Volk
Gemini Observatory, Casilla 603, La Serena, Chile; kvolk@gemini.edu

Bruce J. Hrivnak
Department of Physics and Astronomy, Valparaiso University, Valparaiso, IN 46383; bruce.hrivnak@valpo.edu

and

Sun Kwok
Institute of Astronomy and Astrophysics, Academa Sinica, P.O. Box 23-141, Taipei 106, Taiwan; kwok@asiaa.sinica.edu.tw
Received 2004 July 14; accepted 2004 August 12

ABSTRACT

High-resolution (0.″15) 2.12 μm H_2 and narrowband *K* images have been obtained of one cool proto–planetary nebula, IRAS 20028+3910, and two hot proto–planetary/young planetary nebulae, IRAS 19306+1407 and IRAS 22023+5249. The observations were made with an adaptive optics system and near-infrared imager on the Gemini North 8 m telescope. All three nebulae are seen to be extended, and in two and possibly all three of them H_2 is found to be emitting from bipolar lobes. In IRAS 19306+1407, H_2 emission is seen arising from a ring close to the star and from the edges of emerging bipolar lobes. In IRAS 20028+3910, one bright lobe and a very faint second lobe are seen in the H_2 and *K*-band images, similar to the published visible images, but in the H_2 and *K*-band images a faint filament appears to connect the two lobes. The central star is not seen in IRAS 20028+3910, indicating that the nebula is optically thick even at 2 μm, which is unusual. The images suggest that extended H_2 emission is often the manifestation of fast-slow wind interactions in the bipolar lobes.

Subject headings: circumstellar matter — infrared: ISM — infrared: stars — ISM: lines and bands — planetary nebulae: general — stars: AGB and post-AGB

1. INTRODUCTION

While planetary nebulae (PNe) display a wide range of shapes (circular, elliptical, bipolar, and point-symmetric), asymptotic giant branch (AGB) stars, their progenitors, are observed to be losing mass in a spherically symmetric manner (Neri et al. 1998). This change in the mass distribution appears to be occurring during the transition stage between the two: the proto–planetary nebula (PPN) stage. PPNe consist of a central star of spectral type G through B surrounded by a detached, expanding circumstellar envelope of gas (mostly molecular H) and dust (Kwok 1993).

High-resolution optical images with the *Hubble Space Telescope* (*HST*), which detect scattered light from dust in the circumstellar envelope, show both bipolar and elliptical shapes (Ueta et al. 2000; Su et al. 2001). Since the bipolar nebulae are often nearly edge-on systems, their central stars are often obscured by the dust torus. Those showing elliptical nebular shape could be of truly elliptical shape or could represent bipolar nebulae seen nearly pole-on. In these cases, their central stars are not as obscured and are often visible. Since many of the bipolar PPNe have G–F spectral types, it is apparent that the processes that shape the nebulae are operating by the early part of the PPN phase.

The interacting stellar winds model (Kwok 1982), generalized for the situation in which the circumstellar envelope has an anisotropic density distribution, can explain the general elliptical and bipolar shapes of PNe and PPNe (Balick 1987). Hydrodynamic models have been run that can produce the basic shapes of PPNe (see summary by Frank 1999). The extreme bipolar shapes seen in PPNe, however, suggest that the fast wind may be nonisotropic and highly collimated, therefore allowing the shaping of the nebulae to occur on a much shorter timescale (Kwok 2001).

Emission from excited H_2 provides an opportunity to investigate the initiation and properties of a fast wind from the star that can shape the nebula. H_2 can be excited either radiatively by the UV field of the central star or collisionally by shocks as the wind interacts with the slower-moving detached envelope. By imaging PPNe in H_2, one can determine the presence and location of the excited H_2. However, such observations are not easy, since PPNe and young PNe are small ($\leq 2''$) and require a very high spatial resolution and, in the case in which the central star appears bright, a high dynamic range.

In this study, we have observed three objects that are PPNe or young PNe at high spatial resolution using both a narrowband H_2 filter and a narrowband *K* filter. Some basic properties of the sources are listed in Table 1. All three were discovered to have H_2 emission lines at 2.122 [1–0 *S*(1)], 2.223 [1–0 *S*(0)], and 2.248 [2–1 *S*(1)] μm (D. Kelly & B. Hrivnak 2004, in preparation). Our goals are to determine the spatial location of the H_2 emission, to see how it relates to the method of excitation (collisional or radiative), and, for those that have not previously

[1] The paper is based on observations obtained at the Gemini Observatory with the Adaptive Optics System Hokupa'a/QUIRC, developed and operated by the University of Hawaii Adaptive Optics Group, with support from the National Science Foundation. The Gemini Observatory is operated by the Association of Universities for Research in Astronomy, Inc., under a cooperative agreement with the NSF on behalf of the Gemini partnership: the National Science Foundation (United States), the Particle Physics and Astronomy Research Council (United Kingdom), the National Research Council (Canada), Comisión Nacional de Investigación Científica y Tecnológica (CONICYT; Chile), the Australian Research Council (Australia), Laboratório Nacional de Astrofísica (CNPq; Brazil), and Consejo Nacional de Investigaciones Científicas y Técnicas (CONICET; Argentina).

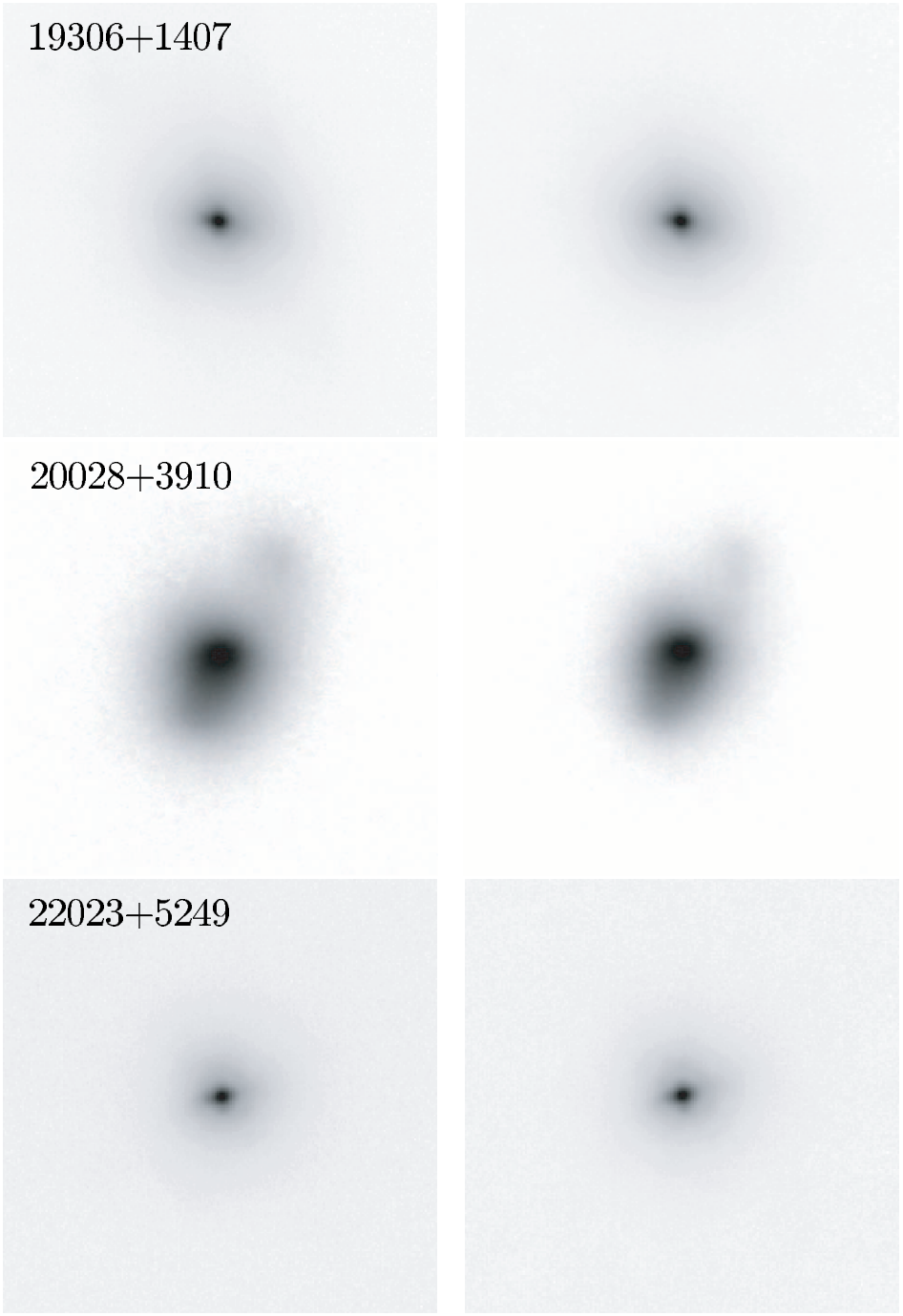

FIG. 1.—Observed 2.12 μm (*left*) and 2.26 μm (*right*) images of the three target objects. To better display the dynamic range, the images of IRAS 19306+1407 and IRAS 22023+5249, which possess bright central stars, are displayed on a square-root scale, and those of IRAS 20028+3910 are displayed on a linear scale. The images are 4.″0 on a side, with north to the top and east to the left.

been imaged at high spatial resolution, to determine the nebular morphology.

2. OBSERVATION AND DATA REDUCTION

Observations were carried out with the University of Hawaii Quick Infrared Camera (QUIRC) near-infrared imager mounted on the exit focus of Hokupa'a at the Cassegrain focus of the Gemini North 8 m telescope. Hokupa'a is a natural guide star adaptive optics system that uses a deformable mirror to correct the wave front (Graves et al. 1998). It produces nearly diffraction-limited resolution at K but requires a bright pointlike source within 30″ of the target. QUIRC uses a 1024×1024 pixel, liquid-nitrogen–cooled HgCdTe array. Mounted with Hokupa'a, it has a fixed plate scale of 0.″020 pixel^{-1}. The pixel size is 18.5 μm, resulting in a field of view of 20.″2. Observations were made through two filters, a narrowband H_2 filter (F212N; $\lambda_c = 2.12$ μm, $\Delta\lambda = 0.023$ μm) and a narrowband K-continuum filter (F226N; $\lambda_c = 2.26$ μm, $\Delta\lambda = 0.060$ μm). The observations were made on 2001 September 17 in the service observing mode. The sky conditions included some thin cirrus.

The observing procedure was as follows. Several (2–5, depending upon brightness) consecutive 60 s observations were made of the targets in each of four different positions, set up in a square dithering pattern with sides of 0.″6. This was done

TABLE 1
PROPERTIES OF TARGETS OBSERVED

IRAS ID	Spectral Type	V (mag)	K (mag)	R.A. (2000.0)	Decl.	l (deg)	b (deg)
19306+1407	Be/young PN	14.2	10.3	19 32 55.1	+14 13 36.9	50.3	−2.5
20028+3910	mid-G	17.8	11.1	20 04 35.0	+39 18 37.9	75.5	+4.2
22023+5249	Be/young PN	12.3	10.7	22 04 11.9	+53 04 02.7	99.3	−2.0

NOTE.—Units of right ascension are hours, minutes, and seconds, and units of declination are degrees, arcminutes, and arcseconds.

through both filters. Then a nearby background field containing a bright star was observed in a similar manner with one or two observations in each position. This nearby bright star can be used to determine the expected point-spread function (PSF) size and shape for the target field, particularly in the absence of a suitable PSF star in the target field. This was necessary in our program since IRAS 22023+5249 had no useful field stars in the small 20″ target image. (IRAS 19306+1407 and IRAS 20028+3910 each had one usable field star.) A United Kingdom Infrared Telescope (UKIRT) faint standard star was also observed for flux calibration (FS 029 = G93-48, $V = 12.74$, $K = 13.31$, spectral type dA3 [Turnshek et al. 1990]). The total exposure time in each filter was 20 minutes for IRAS 19306+1407 and IRAS 20028+3910 and 8 minutes for IRAS 22023+5249.

The images were reduced using standard reduction procedures. They were first dark-subtracted and then flat-field–corrected using dome flats. A general background subtraction was made from all of the F212N and F226N images. The multiple images at each position were combined to remove cosmic rays, and these combined images from the four dithered positions were shifted and median-combined.

This resulted in a 2.12 μm (F212N) image and a narrowband K (F226N) image for each field. These images of the three target objects are displayed in Figure 1. We see that the two filtered images of each target object look basically similar. IRAS 19306+1407 and IRAS 22023+5249 are each dominated by a bright central star, and each appears extended in its outer contours when compared with a star in its field. However, at the lower brightness levels, IRAS 19306+1407 is extended toward the north-northeast and south-southwest of the star in the F212N image but not in the F226N image. IRAS 20028+3910 shows a very interesting morphology, with one bright lobe and a second small, faint lobe opposite it. The central star is not seen; while there is a bright, somewhat peaked region in the brighter lobe, it definitely does not have the profile of a star. The general morphology at 2 μm is similar to that seen in the high-resolution visible *HST* images (Ueta et al. 2000; Su et al. 2001; Hrivnak et al. 2001). For the other two objects, these are the first high-resolution images published.

To distinguish the H_2 emission from the scattered starlight in the lobes and the direct light of the central star, we subtracted a suitably scaled F226N image from the F212N image. The need for scaling arises from several different factors: filter widths and transmission curves, detector response, atmospheric transparency, and spectral shape of the continuum light. To empirically determine the scaling, we first examined the individual target and stellar images in each of our fields. For each target and reasonably bright star in the fields, we measured the FWHM of its radial intensity profile and the peak of a Gaussian function fitted to the profile. These are listed in Table 2. We see that the FWHM was typically about 0.″14 (7.0 pixels), but in two fields (IRAS 20028+3910 and its nearby field) it was almost twice that value. The difference in the FWHM values between the two filters for a particular object is less than 5%, except for three objects that appear wider in the F212N image: the star in the field of IRAS 20028+3910 (20028-S, 7%), the star in the nearby field to IRAS 22023+5249 (22023-NF, 13%), and G93-48 (9%). Thus, the pairs of FWHMs are close enough in width that we did not feel it necessary to artificially broaden one to match the other prior to subtraction. The ratio of the peaks (F212N to F226N) ranges from 0.304 to 0.388, but only for G93-48 is it

TABLE 2
SUMMARY OF THE OBSERVED STAR PROPERTIES

Object[a]	FWHM (2.12) (pixels)	FWHM (2.26) (pixels)	Peak Ratio[b]	Adopted Ratio[c]
19306+1407 (Target)	7.04	7.12	0.380	0.380
19306+1407 (S)	7.19	7.20	0.385	...
19306+1407 (NF)	7.34	7.55	0.388	...
20028+3910 (Target)	30[d]	28[d]	0.342	0.333
20028+3910 (S)	13.52	12.67	0.355	...
20028+3910 (NF1)	15.30	14.58	0.361	...
20028+3910 (NF2)	16.22	16.16	0.374	...
22023+5249 (Target)	6.50	6.65	0.361	0.361
22023+5249 (NF)	8.98	7.87	0.360	...
G93-48 (STD)	6.68	6.11	0.304	...

[a] The designation after the IRAS ID indicates the star measured: Target (PPN/PN), S (star in target field), or NF (star in nearby field).
[b] Ratio of the peaks of the stellar profiles in the two images, in the sense of F212N to F226N.
[c] Ratio used in scaling the F226N image for subtraction from the F212N image for that particular target.
[d] Not a meaningful value, but included to show that it is clearly nonstellar.

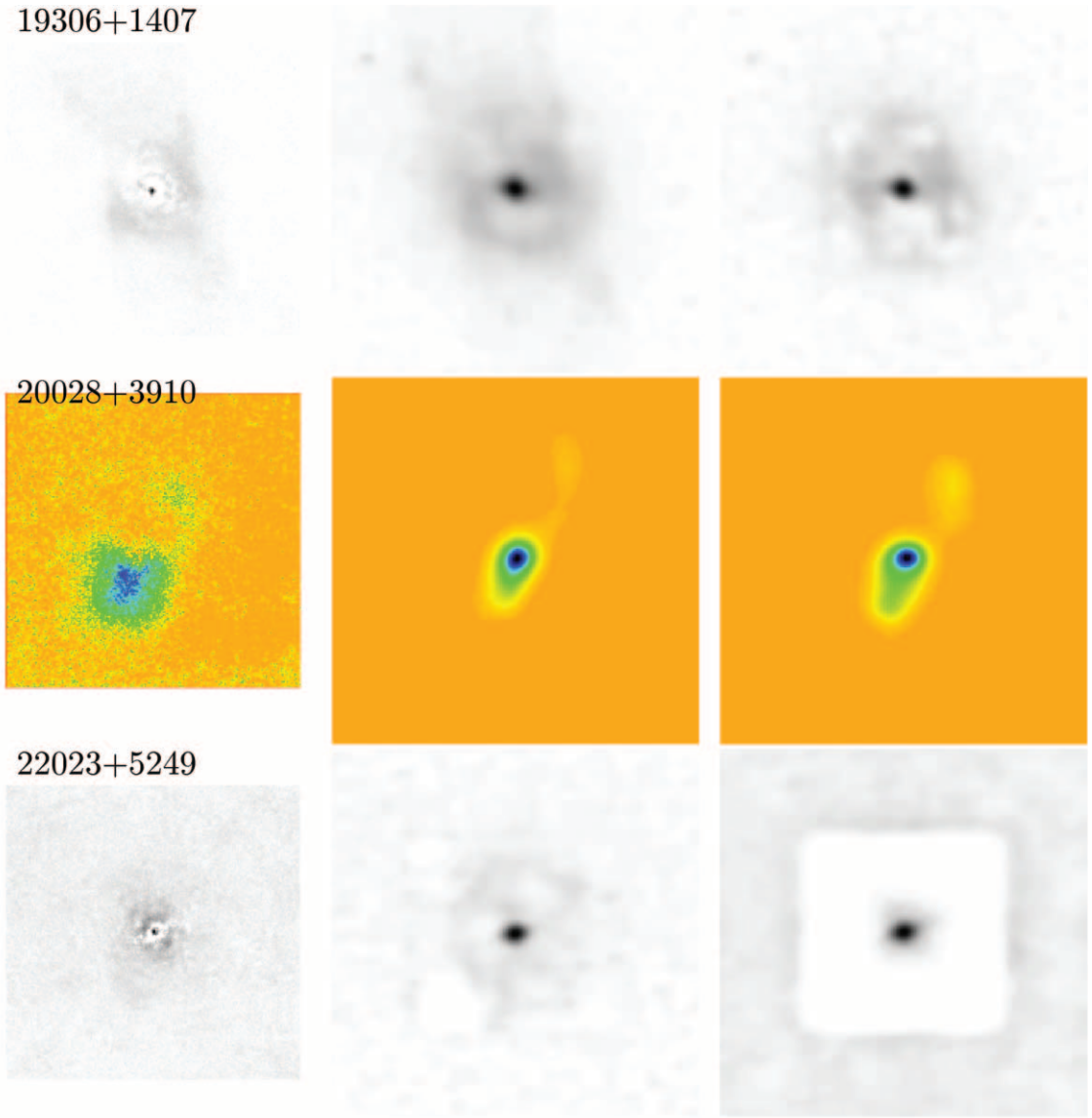

FIG. 2.—Residual H_2 (*left*) and deconvolved 2.12 μm (*center*) and 2.26 μm (*right*) images of the three target objects. The images are all displayed on a linear scale except for the deconvolved images of IRAS 19306+1407 and IRAS 22023+5249, which are on a log scale. False color is used to better display the dynamic range in the images of IRAS 20028+3910. The displayed sizes of the images differ: the H_2 images are 3.″2 on a side, and the deconvolved images are 4.″0 on a side. North is to the top and east to the left. The inscribed square seen in the 2.26 μm and faintly seen in the 2.12 μm images of IRAS 22023+5249 results from the PSF subimage used in the deconvolution.

below 0.34. Excluding G93-48 leads to an average ratio of 0.367 based on all of the other objects and 0.370 excluding the three PPN/PN targets. These are close to the value of 0.38 derived from the simple ratio of filter widths. Since the presence of direct H_2 from the target star would increase this ratio, we began with a scaling ratio for each target based upon the field star in the target image or the nearby-field image. This scaling should effectively remove all of the effects mentioned above, except the difference is spectral shape over the two bandpasses between the field stars and the reflected light from the nebula. However, in two cases we found the targets to have slightly lower ratios; we used these, since they would better represent the spectral shape of the target source. In the third case, we found the ratios to be the same. This suggests that little, if any, of the H_2 emission is coming from the target stars. By thus scaling the ratio to that of the target peaks, we are effectively assuming this to be the case. The adopted ratios are listed in Table 2. The scaled F226N image was then subtracted from the F212N image, and the resulting H_2 images are displayed in Figure 2.

To examine the reality of the resulting H_2 nebulae, we also performed the same exercise on the field stars cited above. While they did not ratio out perfectly, the residual effects were confined to the region close to the peak position of the star ($r \leq 0.''2$, except for one of the fields with a wide FWHM, for which $r \leq 0.''3$) and did not extend out as far as the H_2 lobes found for two of the targets. For these two, we are confident of the reality of the extended H_2 morphology seen in the H_2 images. The results for each target are discussed in the next section.

3. DISCUSSION OF INDIVIDUAL OBJECTS

3.1. *IRAS 19306+1407*

The resulting H_2 image of IRAS 19306+1407 shows that the emission arises primarily from an incomplete ring extending

south of the star and around to the northwest. It appears brightest at two regions of the ring on approximately opposite sides of the star; these could represent limb-brightened edges of the ring. In addition, there is a suggestion of a limb-brightened lobe extending north-northeast of the star and a fainter lobe extending south-southwest of the star. These lobes appear to emerge from the ring along an axis approximately, but not exactly, perpendicular to the two bright regions of the ring.

To further investigate the morphology of the nebula, the F212N and F226N images were slightly deconvolved. The Lucy deconvolution algorithm was used, with the associated field star (Table 2) used as the template star and 20 iterations. These deconvolved images are also shown in Figure 2 but on a logarithmic scale to account for the bright star and faint nebulosity. In the F212N image, a nearly complete ring is seen; we can also more clearly see two limb-brightened lobes emerging from the ring, with that to the north being the brighter. The ring and lobes are absent or much fainter in the F226N image. Taken together, these images support the presence of an H_2-emitting ring around the star that collimates the expanding, limb-brightened, H_2-emitting bipolar lobes that emerge perpendicular to the ring. The ring has a radius of $\sim$0.″7, and the lobes extend $\geq$1.″5 from the star. It appears that the northern lobe is tipped toward us, making this lobe and the southern portion of the ring brighter and the symmetric features somewhat obscured.

The deconvolved F226N image shows some bright regions approximately east and west of the star that correspond approximately to the brighter regions of the ring. In the H_2 image, the region at the position of the star shows a positive residual surrounded by an annulus with a systematically negative residual; this is likely caused by the fact that the FWHM of the target in the F226N image increased slightly when the image was shifted for subtraction. This occurs within the inner 0.″2 of the target image, a region that we have found to be too close to the star to determine reliable information in the subtracted H_2 images (see above).

The 2 μm spectrum of this object (D. Kelly & B. Hrivnak 2004, in preparation) shows, in addition to the three H_2 lines cited in § 1, two additional H_2 emission lines at 2.201 [3–2 S(3)] and 2.154 [2–1 S(2)] μm, the hydrogen Brγ line at 2.166 μm, and a few additional weaker emission lines. Since the width of the slit used in obtaining the spectrum was 2.″6, essentially the entire nebula was included. The location of these lines with respect to the filter profiles is shown in Figure 3. The H_2 line at 2.248 μm falls well within the F226N filter, and the H_2 line at 2.222 μm falls on the wing of the filter. Thus, they will both make some contribution to the flux in the F226N image. If they arise in the same locations as the 2.122 μm line, then their presence in the F226N filter will lower the resulting flux in the subtracted image. We made some calculations using the observed spectrum and the filter profiles to examine these effects. Based upon the relative strengths of the features and the scaling factor, which dilutes the effect of the lines in the F226N image, we estimate that they lower the resulting measured H_2 flux by $\sim$8%, which is within our estimated uncertainty. The unidentified line at 2.138 μm falls within the F212N image, but a calculation shows that its effect is inconsequential. To investigate the expected contribution of the H_2 2.122 μm line to the flux in the F212N image, we integrated the spectrum over the bandpass both with and without the emission line (removed by linear interpolation). The H_2 line of interest is calculated to contribute $\sim$9% of the F212N flux. This compares favorably to the value of $\sim$7% determined by comparing the fluxes of the resulting H_2 image with the F212N image. We regard this as a good confirmation that we have properly removed the scattered light continuum in deriving the H_2 image.

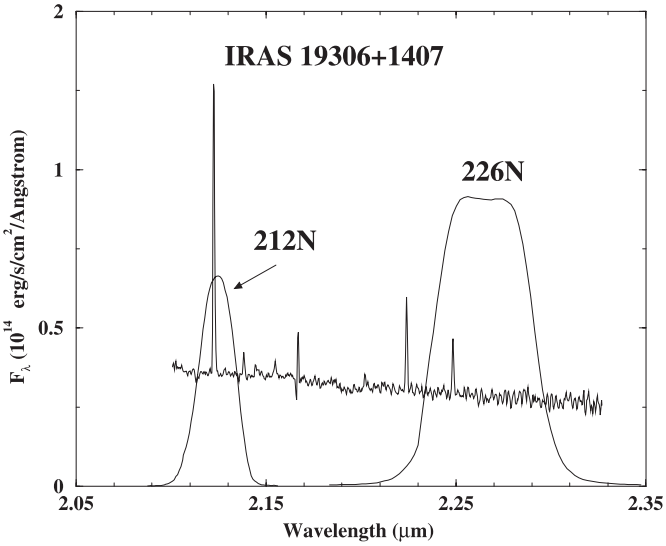

FIG. 3.—Plot of the 2 μm spectrum of IRAS 19306+1407 (D. Kelly & B. Hrivnak 2004, in preparation) with the profiles of the F212N and F226N filters overplotted.

IRAS 19306+1407 is associated with a medium-bright (V = 14.2 mag) star. Recent *HST* visible-band imaging shows a bipolar structure with elongated lobes that looks very similar in morphology to our deconvolved F212N image (R. Sahai 2004, private communication). Our optical spectrum shows an early B spectral type (B0:) with Hα and Hβ in emission along with [N II] lines. A high-resolution spectrum of the Hα line reveals wide wings indicating a high-velocity outflow (Sahai & Sánchez Contreras 2004). Its mid-infrared spectrum was observed with the *Infrared Space Observatory* (*ISO*) and showed the emission features at 3.3, 6.2, and 7.7 μm commonly seen in hot carbon-rich objects such as planetary nebulae (Hrivnak et al. 2000). Based upon these features and the shape of the mid-infrared spectrum, Hrivnak et al. (2000) suggest that it may be a young PN. Note that the statement by García-Lario et al. (1997) that "the optical counterpart corresponds to a faint K-type star with no emission lines 9″ north and 42″ east of a bright ($m_v \sim 13$) star" is incorrect. CO (Likkel et al. 1991), OH, and H_2O (Likkel 1989) observations of this source have failed to detect line emission.

3.2. *IRAS 20028+3910*

We determine that the H_2 emission is coming from the two lobes seen in these new 2 μm images, with the same basic morphology as seen in scattered light. This is shown in Figure 2. There appears to be a faint filament connecting the fainter lobe with the brighter one. We note that in this case we needed to decrease the scale factor to 0.333 to avoid a systematic hole of negative flux in the center. While this is a smaller value than that determined for the other objects, we attribute it to the much redder color of this source, which changes the slope of the continuum over the 2 μm region as compared with the other sources. To investigate this further, we calculated for all three targets the expected flux ratio of the two filters based only upon the observed spectra and the filter profiles and found the ratio for IRAS 20028+3910 to be 0.03 lower than that for the other two target objects. This is consistent with what we find here.

We proceeded to deconvolve the F212N and F226N images using the Lucy algorithm with 20 iterations. These deconvolved images are also seen in Figure 2; note that a logarithmic scale is used. A filament can be seen on the west side connecting the brighter and fainter lobes, similar to that seen in the H_2 image. A bright ridge runs the length of the southern lobe with a peak in brightness near the northern end. However, this peak does not have a stellar profile, and the nebula appears to be optically thick at this wavelength.

The 2 μm spectrum of this object shows no additional features beyond the three H_2 lines cited in § 1. Examining the contribution of these lines to the flux in the two images, as was done for IRAS 19306+1407, we find that their presence in the F226N image has the effect of reducing the resulting H_2-subtracted flux by $\sim$10%, again within our uncertainties. Based upon the observed spectrum convolved with the filter profile, we calculate that the H_2 line contributes $\sim$5% of the flux in the F212N image. That is in good agreement with the value of $\sim$6% we determine from our H_2 image.

IRAS 20028+3910 is faint in visible light ($V = 17.8$), and a low-resolution optical spectrum suggests a mid-G spectral type. The mid-infrared *ISO* spectrum is that of a featureless red source. CO line emission has been detected in this source (Likkel et al. 1991), but a detection of HCN is uncertain (Omont et al. 1993). This object appears to be a bipolar PPN, but the nature of the circumstellar chemistry (carbon- or oxygen-rich) is as yet undetermined; however, based upon its mid-infrared spectrum, it is likely to be carbon-rich.

3.3. *IRAS 22023+5249*

The resulting H_2 image of IRAS 22023+5249 shows emission arising from two opposite sides of the star at a radial distance of $\sim$0.″2. The central portion shows a positive peak at the position of the star surrounded by a negative ring of radius $\sim$0.″08, a pattern that can arise if the object in the F212N image is slightly narrower. The total flux very close to the star ($r \sim$ 0.″1) integrates to zero. Thus it appears that H_2 emission arises close to the star in two small bipolar regions oriented northeast and southwest of the star, with the northeast lobe slightly brighter. However, because of the small size of the emission region, we are cautious in putting too much confidence in the bipolar pattern. Deconvolution was carried out on the F212N and F226N images. The F212N image reveals a number of H_2 knots lying at approximately 0.″7 from the star, forming a somewhat circular pattern. These are not seen in the F226N image, which shows only a little nebulosity close to the star. However, these results are somewhat compromised because the PSF star came from the nearby field and not the same image as the PPN. We conclude for IRAS 22023+5249 that the H_2 emission, which is surely present as demonstrated by the spectrum, arises in a region close to the star ($r \sim 0.''2$) and perhaps also in a clumpy ring of radius $\sim$0.″7.

The 2 μm spectrum of this object (D. Kelly & B. Hrivnak 2004, in preparation) shows, in addition to the three H_2 lines cited in § 1, the two additional H_2 emission lines and the Brγ line as seen in IRAS 19306+1407 and several additional weaker emission lines. In this case, the consequence of these H_2 lines in the F226N image would be to lower the resulting H_2 flux by $\sim$14%. The contribution of the 2.212 H_2 line to the F212N image is computed to be $\sim$9%; this is in good agreement with the value we determine from our H_2 image of $\sim$8%.

IRAS 22023+5249 is associated with a bright ($V =$ 12.3 mag) star (LS III +52°24). An optical spectrum shows a B spectral type with hydrogen emission lines Hα and Hβ. García-Lario et al. (1997) state that it shows the presence of low-excitation nebular emission lines, and, on this basis and the detection of radio continuum emission (they cite M. Ratag 1991, private communication), they identify it as a new planetary nebula. Thus, IRAS 22023+5249 is likely an object making the transition from the end of the PPN to the young PN stage. CO (Omont et al. 1993) observations of this source have failed to detect line emission.

4. DISCUSSION OF RESULTS

Kastner et al. (1996) have found a correlation between bipolar PNe and H_2 emission in the sense that most bipolars have H_2 emission; in these cases the strongest H_2 emission is usually observed to emanate from the waist region between the lobes. They also find that the PNe with H_2 are systematically located at lower galactic heights, which suggests that they are more common in stars of higher mass. However, D. Kelly & B. Hrivnak (2004, in preparation) found that probably all PPNe (or young, very low excitation PNe) with B central stars display H_2 emission. It appears that at this temperature the star has become hot enough to produce the required UV photons to excite the molecule. The H_2 emission seen later in the PN evolution appears to depend, then, on shielding by dust or H_2 self-shielding in an equatorial disk.

Both IRAS 19306+1407 and IRAS 22023+5249 are B stars in the process of becoming young PNe. On the basis of H_2 line ratios, it has been determined that the H_2 is mostly radiatively excited in IRAS 22023+5249 and partly radiatively excited in IRAS 19306+1407 (D. Kelly & B. Hrivnak 2004, in preparation), consistent with the increase in the UV radiation field in these objects. However, the H_2 emission from IRAS 19306+1407 is primarily collisionally excited. On the basis of these new images, it appears that the wind is impacting on a dense torus around the star and emerging in bipolar lobes formed as the wind interacts with the circumstellar envelope. As this star evolves to higher temperatures, it may be only the H_2 emission from the torus that remains.

D. Kelly & B. Hrivnak (2004, in preparation) found that among F and G spectral type PPNe, the only ones in which H_2 emission was seen possessed a bipolar morphology. Their study included IRAS 20028+3910, and they based the morphological classification of the object on the visible image. Here we see that it has a similar appearance in the H_2 emission and *K*-band filters. The H_2 emission in this object was found to be collisionally excited, consistent with the other F−G PPNe with H_2 emission.

For IRAS 20028+3910, the star is not seen at 2 μm even though the inclination of the polar axis to the line of sight is estimated to be $\sim$30° (Su et al. 2001). This suggests a very high optical depth, reminiscent of the Egg Nebula (AFGL 2688), in which the central star also is not seen in the near-infrared (Sahai et al. 1998a; Weintraub et al. 2000) and the equatorial disk is optically thick out to $\sim$30 μm (Lopez & Perrin 2000). A simplified, spherically symmetric model of the circumstellar shell of IRAS 20028+3910, assuming amorphous carbon and adjusted to fit the spectral energy distribution, indicates an optical depth of 1.2 toward the central star at 11 μm. The H_2 emission from the Egg Nebula and IRAS 17150−3224 is excited collisionally, and this is the primary excitation mechanism in IRAS 20028+3910 (D. Kelly & B. Hrivnak 2004, in preparation), perhaps as the fast wind interacts with the circumstellar envelope along the lobes. All three of these PPNe have central stars with F−G spectral types, bipolar lobes with an obscuring lane across the waist, two pairs of oppositely

pointed "searchlight beams" that appear to originate at the location of the central star, and concentric circumstellar arcs (Sahai et al. 1998b; Kwok et al. 1998; Hrivnak et al. 2001). (IRAS 17150−3224 differs from the other two in that its central star is visible in the near-infrared [Su et al. 2003] and it has silicate dust.) The fact that IRAS 20028+3910 is optically thick at 2 μm prohibits us from determining the location of the H_2 emission; it can arise close to the star or anywhere within the lobes.

In IRAS 19306+1407, H_2 emissions are seen in both the bipolar lobes and the equatorial ring. This structure resembles the Egg Nebula, in which H_2 emissions are prominent in both the lobes and the torus (Cox et al. 1997; Sahai et al. 1998b). We need to remember that the observed bipolar lobes seen in visible light in PPNe such as the Egg Nebula and IRAS 17150−3224 do not represent the physical distribution of matter, but in fact represent cavities from which scattered light can escape. The fact that the H_2 emission in PPNe is seen in the lobes is not surprising, because the H_2 emission traces the wind interaction and is expected to be strongest along the edges of the interaction cones. The origin of the H_2 emission seen in the ring is less clear; it may result from the interaction between the equatorial torus and an earlier spherical slow wind, or it may be the result of multiple collimated bipolar outflows (Cox et al. 2000). In the case of the Egg Nebula, at least three pairs of point-symmetric bipolar outflows are evident in the equatorial regions. The fact that we see a more ringlike structure in IRAS 19306+1407 does not preclude a similar intrinsic structure to that of the Egg Nebula, but may just be the result of a different orientation and a weaker signal-to-noise ratio. It is not inconceivable that a deeper image taken from space (e.g., with the *James Webb Space Telescope*) may reveal similar multipolar structures in IRAS 19306+1407.

H_2 images have previously been published for only a few PPNe. These reveal that the H_2 emission arises primarily within the bipolar lobes. It may arise in the ends of the lobes, as in AFGL 2688 (F5 Ia; Sahai et al. 1998a), Rob 22 (A2 I; Sahai et al. 2000), and IRAS 17150−3224 (G2 I; Su et al. 2000), or from the edges of the lobes, as in Hen 401 (B0 I; Sahai et al. 2000). In this study, H_2 emission is found to arise in a ring and along the edges of bipolar lobes in IRAS 19306+1407 (B0). In IRAS 20028+3910 (∼G4), the emission also arises in the bipolar lobes, although the exact location cannot be determined since the lobes are optically thick at this wavelength.

5. SUMMARY AND CONCLUSIONS

Ground-based, high-resolution ($R \sim 0\farcs15$), near-infrared images of one cool PPN and two objects making the transition to young PNe are presented. For one of these young PNe, the H_2 emission source is clearly resolved as a circumstellar ring (torus) and bipolar lobes; for the second one, it is seen to arise close to the star, perhaps in a bipolar morphology and perhaps also in a surrounding ring. For the cool PPN, the nebular lobes are clearly seen in scattered light, and the H_2 emission arises in the lobes, although its exact source cannot be determined because the lobes are optically thick in the *K* band. These three raise the number of PPNe imaged in H_2 at high resolution ($\leq 0\farcs2$) to seven and show that the H_2 emission arises primarily in the bipolar lobes or in the equatorial torus (at least in those that are collisionally excited). H_2 imaging of PPNe therefore represents an excellent method to trace the wind interactions, particularly in cases of multipolar outflows such as could be occurring in IRAS 19306+1407.

These observations effectively demonstrate the high spatial resolution obtainable in the near-infrared with a large ground-based telescope and adaptive optics. The resolution is comparable to that obtained with the Near-Infrared Camera and Multi-Object Spectrometer (NICMOS) on the *HST*, and these kinds of observations will be increasingly important as the lifetime of the *HST* draws to a premature conclusion.

We thank K. Roth, T. Davidge, O. Guyon, and P. Baudoz, who carried out the observations. B. J. H. acknowledges support for this work from the National Science Foundation under grant AST-9900846, and S. K. and K. V. acknowledge grants from the Natural Science and Engineering Research Council of Canada.

REFERENCES

Balick, B. 1987, AJ, 94, 671
Cox, P., et al. 1997, A&A, 321, 907
———. 2000, A&A, 353, L25
Frank, A. 1999, NewA Rev., 43, 31
García-Lario, P., Manchado, A., Pych, W., & Pottasch, S. R. 1997, A&AS, 126, 479
Graves, J. E., Northcott, M. J., Roddier, F. J., Roddier, C. A., & Close, L. M. 1998, Proc. SPIE, 3353, 34
Hrivnak, B. J., Kwok, S., & Su, K. Y. L. 2001, AJ, 121, 2775
Hrivnak, B. J., Volk, K., & Kwok, S. 2000, ApJ, 535, 275
Kastner, J. H., Weintraub, D. A., Gatley, I., Merrill, K. M., & Probst, R. G. 1996, ApJ, 462, 777
Kwok, S. 1982, ApJ, 258, 280
———. 1993, ARA&A, 31, 63
———. 2001, in Post-AGB Objects as a Phase of Stellar Evolution, ed. R. Szczerba & S. K. Gorny (Dordrecht: Kluwer), 3
Kwok, S., Su, K. Y. L., & Hrivnak, B. J. 1998, ApJ, 501, L117
Likkel, L. 1989, ApJ, 344, 350
Likkel, L., Forveille, T., Omont, A., & Morris, M. 1991, A&A, 246, 153
Lopez, B., & Perrin, J. M. 2000, A&A, 354, 657
Neri, R., Kahane, C., Bujarrabal, V., & Loup, C. 1998, A&AS, 130, 1
Omont, A., Loup, C., Forveille, T., te Lintel Hekkert, P., Habing, H., & Sivagnanam, P. 1993, A&A, 267, 515
Sahai, R., & Sánchez Contreras, C. 2004, in ASP Conf. Ser. 313, Asymmetrical Planetary Nebulae III, ed. M. Meixner et al. (San Francisco: ASP), 32
Sahai, R., Su, K. Y. L., Kwok, S., Dayal, A., & Hrivnak, B. J. 2000, in ASP Conf. Ser. 199, Asymmetrical Planetary Nebulae II, ed. J. H. Kastner, N. Soker, & S. A. Rappaport (San Francisco: ASP), 167
Sahai, R., et al. 1998a, ApJ, 492, L163
———. 1998b, ApJ, 493, 301
Su, K. Y. L., Hrivnak, B. J., & Kwok, S. 2001, AJ, 122, 1525
Su, K. Y. L., Hrivnak, B. J., Kwok, S., & Sahai, R. 2003, AJ, 126, 848
Su, K. Y. L., Kwok, S., Hrivnak, B. J., & Sahai, R. 2000, in ASP Conf. Ser. 199, Asymmetrical Planetary Nebulae II, ed. J. H. Kastner, N. Soker, & S. A. Rappaport (San Francisco: ASP), 163
Turnshek, D. A., Bohlin, R. C., Williamson, R. L., II, Lupie, O. L., Koornneef, J., & Morgan, D. H. 1990, AJ, 99, 1243
Ueta, T., Meixner, M., & Bobrowsky, M. 2000, ApJ, 528, 861
Weintraub, D. A., Kastner, J. H., Hines, D. C., & Sahai, R. 2000, ApJ, 531, 401